

# Contracting Skeletal Kinematics for Human-Related Video Anomaly Detection

Alessandro Flaborea<sup>a,1,\*</sup>, Guido Maria D'Amely di Melendugno<sup>a,1</sup>, Stefano D'Arrigo<sup>b,1</sup>, Marco Aurelio Sterpa<sup>b</sup>, Alessio Sampieri<sup>b</sup>, Fabio Galasso<sup>a</sup>

<sup>a</sup>*Department of Computer Science, Sapienza University of Rome, Italy*

<sup>b</sup>*Department of Computer, Control and Management Engineering, Sapienza University of Rome, Italy*

---

## Abstract

Detecting the anomaly of human behavior is paramount to timely recognizing endangering situations, such as street fights or elderly falls. However, anomaly detection is complex since anomalous events are rare and because it is an open set recognition task, i.e., what is anomalous at inference has not been observed at training. We propose COSKAD, a novel model that encodes skeletal human motion by a graph convolutional network and learns to COntract SKeletal kinematic embeddings onto a latent hypersphere of minimum volume for Video Anomaly Detection. We propose three latent spaces: the commonly-adopted Euclidean and the novel spherical and hyperbolic. All variants outperform the state-of-the-art on the most recent *UBnormal* dataset, for which we contribute a *human-related* version with annotated skeletons. COSKAD sets a new state-of-the-art on the human-related versions of *ShanghaiTech Campus* and *CUHK Avenue*, with performance comparable to video-based methods. Source code and dataset will be released upon acceptance.

*Keywords:* anomaly detection, open set recognition, hyperbolic geometry, kinematic skeleton, graph convolutional networks

---

\*Corresponding author

*Email address:* flaborea@di.uniroma1.it (Alessandro Flaborea)

<sup>1</sup>The first three authors contributed equally.

## 1. Introduction

Anomaly Detection (AD) is a broad and well-studied field in computer vision, which aims to detect events that deviate from normality automatically [1]. More precisely, the task is to detect anomalous events in footage and label the corresponding frames as abnormal. AD is a complex and multifaceted field with applications beyond just video surveillance [2]. Many techniques have been successfully applied in several real-world scenarios, including monitoring elderly individuals [3], industrial systems [4] and social networks [5].

While significant progress has been made in AD in recent years, this task still presents several challenges: (1) anomalous events are rare in real-world scenarios, and this reflects in the imbalanced distribution of normal and anomalous events in public AD datasets. (2) Anomalous events are challenging to identify since abnormal actions can involve either frenetic movements (e.g., fights) or very still postures (e.g., faints), resulting in a context-dependent definition of anomaly, which varies among public datasets. Furthermore, the same anomalous action can vary significantly among individuals, adding to the intra-class variation that must be considered. Finally, (3) when working with videos of humans, it is crucial to consider privacy and fairness concerns, such as avoiding violations of individuals’ rights or exploiting social biases.

In this work, we propose COSKAD. This novel end-to-end model infers abnormality COnttracting SKeletal (COSKAD) embeddings in the latent space and opens up a novel investigation of the latent metric space encoding the regular motions. The proposed method tackles all the limitations mentioned above. First, it adheres to the *One-Class-Classification* (OCC) [6, 7, 8, 9, 10] protocol, which simulates the scarcity of abnormal events exposed in (1). Moreover, COSKAD exploits the compact spatio-temporal skeletal representation (cf. Fig. 1) of human motion instead of raw frames, typically employed with video-based methods. This modality comes with several advantages; first, recent work [11] in the motion-related fields of Pose Forecasting and Action Recognition has proven the superiority of this modality with respect to the raw video frames for mo-

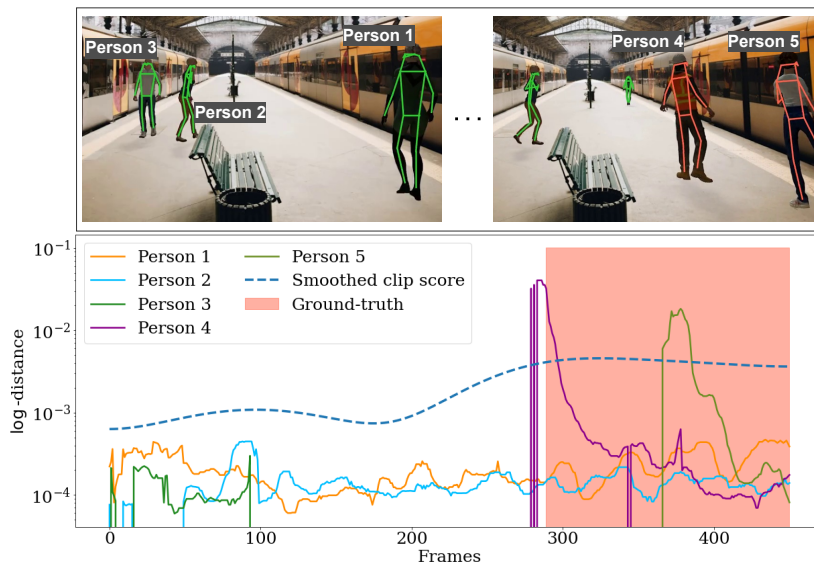


Figure 1: Anomaly score provided by COSKAD on a clip from the UBnormal dataset. COSKAD correctly classifies the motion of the two staggering characters (red skeletons in the upper-right picture) in the last part of the clip as anomalous.

tion representation. Exploiting this input modality, our proposed model is more robust to slight motion deformations that represent the intra-class variability described in (2) while preserving the ability to distinguish between different actions, e.g., walking vs. running, which is crucial in AD. Furthermore, modeling agents as kinematic graphs allows for separating the person detection task (handled as a preprocessing step) from the anomaly detection task, resulting in a more computationally efficient and context-agnostic method. Although skeletal representations are more compact than raw video frames, they contain the necessary information for effectively characterizing motions, as demonstrated by the state-of-the-art results of skeleton-based methods [8, 9, 10]. Finally, the skeletal representation is more privacy-preserving (3) since it ignores biometric details, representing all samples with anonymous tensors of coordinates. Consistently with this setting, we adopt the Human Related (HR)[9] split of the datasets, which corresponds to a version of the dataset that admits only anomalies gener-

ated by humans, e.g., people fighting, disregarding anomalies coming from the context scene, e.g., a car proceeding on the pavement.

The proposed model comprises two founding components: an encoder and a projector module. Differently from previous related works, which use either ST-GCN [10, 12, 13], or a Recurrent Neural Network [9] to encode the human motion, COSKAD implements its encoder as a Space-Time-Separable Graph Convolutional Network [14]. As far as we know, this is the first study to adapt it for skeletal-based AD and to expose a comparison among different GCN-based encoders (presented in Sec. 5.1). The projector module draws inspiration from SSL, where it has been shown to play a crucial role [15, 16], which we confirm here in detailed ablation studies (cf. Sec. 5.2). Finally, we define a data-driven metric objective in the latent space to minimize the distance between the skeletal embeddings and a center. We call the distance minimization *contraction*, as it forces normality to concentrate around an origin. Dealing with a metric objective, we further propose a novel investigation of how the latent distribution might be altered, condensed, or expanded using the peculiar metric properties of three distinct manifolds: the Euclidean ( $\mathbb{R}^n$ ), the hyperbolic space ( $\mathbb{H}^n$ ), and the n-Sphere ( $\mathbb{S}^n$ ). As far as we know, this is the first work to have studied different latent spaces for skeleton-based anomaly detection. The proposed model is simple, lightweight, and effective, as we illustrate in extensive experiments, where COSKAD outperforms state-of-the-art (SoA) models (including some video-based techniques) on three challenging benchmarks: *HR-ShanghaiTech Campus* [10, 13], *HR-Avenue* [9, 17], and the recent *UBnormal* [18].

Additionally, we offer an ablative examination of several of our model’s key features. Beyond a thorough ablation study on the main modules of our proposed COSKAD, we also compare the encoder-based architecture proposed with an autoencoder and compare two alternative strategies to define the hypersphere center, extending the seminal study of [19]. Finally, we propose a novel HR version of *UBnormal* [18], dubbed *HR-UBnormal* as an additional contribution. We create *HR-UBnormal* by filtering out anomalous events that do not involve

human individuals, e.g., we remove scenes of fire and car accidents unless people are involved. We leverage an established Pose Estimator [20] and refine its results with a Pose Tracker [21] to extract human poses in each UBnormal’s video frame. So, HR-UBnormal contains human-related anomalies and human skeletons at all frames, inspected for accuracy and temporal consistency. To summarize, the contribution of this paper is threefold:

- We introduce COSKAD, a simple, end-to-end, and effective model that surpasses SoA results on three public benchmarks.
- We conduct an in-depth study on three different manifolds as latent spaces and explore their intrinsic properties, and thoroughly analyze their effects on our novel AD system.
- We introduce a new *HR* version of UBnormal with a filtered selection of clips featuring human-related events and an extended set of human body pose annotations.

## 2. Related work

Anomaly Detection (AD) is a multi-faceted field with applications in several domains (see [22, 23] for surveys). This work focuses on skeleton-based anomaly detection, a type of video-based AD that involves analyzing the movements and poses of human bodies in a video. In this section, we compare works that most closely relate to ours, distinguishing error-based and score-based video AD techniques and skeleton-based models.

### 2.1. Video AD

Early proposed methods analyze the trajectories of agents in the video to unearth those that differ from normality [24, 25]. More recent deep learning methods for Video AD can be roughly collected into two categories: error-based or score-based.

**Error-based methods.** These methods attempt to detect anomalies through a generative process in which a model produces new video frames, which are then compared with ground truth. These methods assume that a model trained with only normal data will struggle to generate the anomalous frames, producing a more significant error that can be directly used as the anomaly score. [6] used convolutional AutoEncoder (AE) and defined the input volume as a stack of sequential grayscale frames. [26] during the training phase builds a memory of the most representative normal poses. During the inference phase, for each sample, it finds the most similar example in memory and estimates its ground truth distance. Unlike these methods, COSKAD relies on a GCN-encoder, an ideal tool for exploring relationships between body joints over time in the kinematic graph and extracting semantically consistent latent embeddings.

**Score-based methods.** These approaches have been extensively studied [19, 27, 28]. They derive abnormality in videos by monitoring some quantity extracted from the embeddings produced by the deep network. For example, [29] proposed a two-stage method in which videos are divided into cubic patches and first analyzed with Gaussian classifiers to exclude the least relevant patches, e.g., background. Then, the remaining candidates are processed by a more complex CNN. In contrast, COSKAD looks at the latent space positions occupied by input embeddings to derive clues of abnormality. While working with images rather than video, Deep Support Vector Data Description (DSVDD) [19] and OC4Seq [28] are two methods related to COSKAD, as both employ a DSVDD objective seeking to minimize a sphere enclosing the generated embeddings. While we also employ an SVDD objective, our model learns in an end-to-end way to map the representation of the normal samples in the latent space while encoding semantic representations thanks to its separable GCN encoder. As far as we know, this work is the first to propose the SVDD objective for Video AD with skeleton-based representations.

## 2.2. Skeleton-based AD

[9] first introduces the skeleton-based representation in AD; their method

presents a two-branches architecture for reconstruction and forecasting modeled as GRUs. [8] sets up the problem as motion forecasting and defines their model by stacking layers of ST-GCN [12] followed by an MLP forecasting module. While they introduce the use of GCN, the adjacency matrix is fixed and does not allow the exploration of intra-frame and intra-joint relationships, improving spatio-temporal features encoding [14]. [10] proposes a two-stage network in which they train an autoencoder (built on ST-GCN [12]), and, in the second stage, it clusters the produced embeddings in the latent space. These clusters should represent the normality styles in the train set, but it is challenging to spot the optimal number of clusters. Differently, COSKAD has an end-to-end approach and solves the problem of the number of clusters by forcing the entire train set into the same latent region, constraining the distances to a common center.

### 3. Methodology

In this section, we describe our proposed model focusing on its modules and the steps taken to train and assess it.

We assume the human body kinematics to be available as skeleton representations for a few given frames (cf. Sec. 4.1.1 for the details on the skeleton sequence extractions for the proposed HR-UBnormal dataset). These spatio-temporal graph inputs are fed to COSKAD which, as illustrated in Fig. 2, relies on two key components: a separable graph encoder and a projection module. The encoder processes the input graph and produces embeddings representing the motion of each individual. The projector adapts the embedding provided by the encoder for the mapping in the latent space. Both modules are jointly trained with a spatial minimization objective, which aims to catch the correspondences among samples belonging to the same class. Finally, we define a novel metrical objective in the latent space in order to guide the training and consider three different manifolds as latent spaces: the *Euclidean Space* ( $\mathbb{R}^n$ ), the *Poincaré Ball* ( $\mathbb{D}^n$ ), and the *n-Sphere* ( $\mathbb{S}^n$ ), to inherit their specific metric

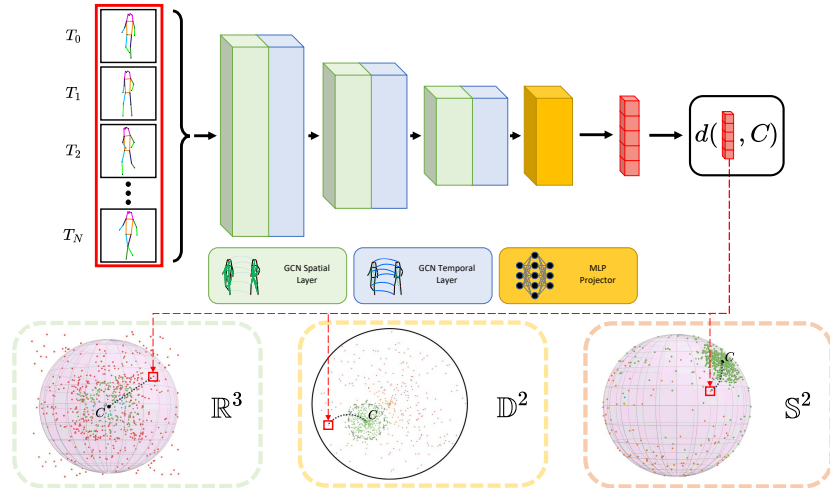


Figure 2: The overall architecture of COSKAD. The model combines an STS-GCN-based [14] encoder (light green and light blue blocks) with a projector module (yellow block). After projection, the latent representation (red vector in the figure) is embedded into the latent space. We propose and evaluate 3 variants of the latent space: *Euclidean*  $\mathbb{R}^n$ , *spherical*  $\mathbb{S}^n$ , and the *hyperbolic* modeled with the Poincaré Ball  $\mathbb{D}^n$ . During training, the embeddings are constrained to accumulate in a narrow region in the chosen manifold by reducing the distance between the motion embedding and the common center. The sequences mapped further from the center are interpreted as anomalous during inference.

properties.

**Formulation.** The motion trajectories consist of  $V$  joints per actor in each frame tracked across all the frames ( $T_{actor}$ ) where the actor is present. We apply a temporal sliding window crop on the trajectories to get sequences of  $V$  joints' spatial positions for  $T$  adjacent time frames. Finally, we organize the input signal as a graph  $\mathcal{G} = (\mathcal{V}, \mathcal{E})$ , with  $TV$  nodes  $x_i \in \mathbb{R}^C$ , where  $C = 2$  stands for the  $x, y$  joint coordinates, and with edges  $(i, j) \in \mathcal{E}$ , represented by a spatio-temporal adjacency matrix  $A^{st} \in \mathbb{R}^{VT \times VT}$ , relating all joints to all others across all observed time frames.

### 3.1. Encoder and Projector module

We encode the body kinematics of a person with a SoA variant [14] of Graph Convolutional Network (GCN) [30]. GCNs are the go-to choice in the kinematic-related fields of Pose Forecasting [11, 14, 31] and action recognition [12, 32]. COSKAD leverages a separable GCN-encoder designed to capture spatio-temporal signals and produce consistent features. Specifically, the encoding performs a factorization of the adjacency matrix  $A$  into two learnable submatrices  $(A_s, A_t)$  responsible for spatial and temporal interconnections, respectively.  $A_s \in \mathbb{R}^{T \times V \times V}$ , the *spatial adjacency matrix*, learns the relationships between different joints in each frame by learning their interdependence. In contrast,  $A_t \in \mathbb{R}^{V \times T \times T}$ , the *temporal adjacency matrix*, deals with the connections between different temporal instants for each joint.

This strategy, also adopted by [14] in the context of pose forecasting, ensures effective encoding of the spatio-temporal features of the input graph by learning and exploiting the joint-joint and time-time relationships that characterize human motion. In addition, this factorization results in a considerable reduction in the number of parameters ( $\sim 4x$  with respect to a plain GCN) since it does not consider the relationships between different joints in different frames.

We formulate a single encoder layer as:

$$X^{l+1} = \sigma(A_s A_t X^l W) \quad (1)$$

where  $X^l$  is the input from the previous layer,  $W \in \mathbb{R}^{C \times C'}$  are learnable weights and  $\sigma$  an activation function. We stack four separable GCN layers interleaved with residual connections to encode the entire input sequence. Overall, the results of our ablation studies (cf. Sec. 5.1) suggest that the separable GCN is the best encoder among the GCN architectures we evaluated.

Reminiscent of recent works in Self-Supervised Learning (SSL) [15, 16], we explicitly define a projector module to refine the Encoder representation and accommodate it in the latent space. The projector comprises two identical blocks that iteratively process their input with a Fully Connected Module followed by a

ReLU non-linearity and a Batch Normalization [33] layer. Despite its simplicity, we found it beneficial to add this module, as shown in Sec. 5.2.

### 3.2. Objective

The OCC formulation requires that the train sets contain elements of a single class. Therefore, the design of the objective function is crucial, as it can only exploit the similarities that normal samples exhibit. Many existing methods [7, 8, 9, 26] formulate the anomaly score using a proxy task, such as the reconstruction error. In Sec. 5.4, we experimentally confirm that this is suboptimal, as maintained in [34], since it does not align directly with the inference AD objective.

In this work, we define a metric objective that encourages the model to arrange the train samples in a narrow region in the latent space: inspired by [19], the objective is defined as:

$$\min_{\mathcal{W}} \frac{1}{N} \sum_{i=1}^N d(\Phi(x_i, \mathcal{W}), c) + \alpha f(\mathcal{W}) \quad (2)$$

Where  $\Phi$  represents the mapping in the latent space defined by COSKAD,  $\mathcal{W}$  is the set of its parameters,  $x_i \in \mathbb{R}^{T \times V \times C}$  is an input sample,  $d$  is a metric defined in the latent space,  $f$  is a weight decay regularizing function, and  $c$  is the center of the hypersphere. We follow [19] and initialize  $c$  by taking the average of the final embeddings after an initial forward pass. Then, [19] suggests training the model with the parameter  $c$  fixed. We argue that this practice may harm the training, leading to a non-optimal solution since the center is precalculated and its position does not evolve with the learning.

Differently from [19], we introduce a novel and more tailored data-driven dynamic for the center: at the beginning of each training epoch, the position of the center is refined to be the centroid of the data’s projection in the latent space. The benefit of this moving center is twofold. First, a data-driven center relieves the encoder and the projector learning not being constrained to accumulate projection around a fixed point. Secondly, it encourages COSKAD to explore the latent space to find a region that accommodates the representations, which

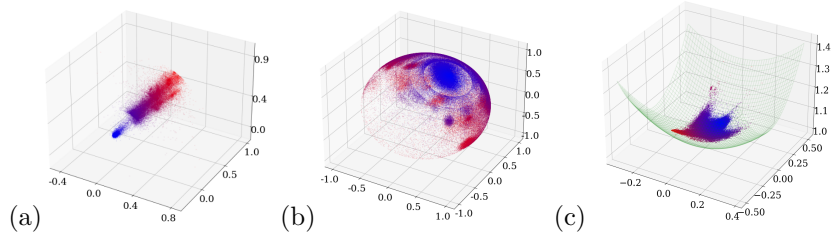


Figure 3: Visualization of the UBnormal test set’s latent vectors embedded in three different manifolds: (a) Euclidean, (b) spherical, and (c) hyperbolic. We retain the three dimensions with the highest variance and color-code the points according to their distance from the center, from blue (closest) to red (furthest). Distance is intended as the  $L^2$  norm in the Euclidean case, the *cosine distance* on  $\mathbb{S}^n$ , and the *Poincaré distance* for the hyperbolic embeddings. In the hyperbolic case, we highlight in green the hyperboloid onto which the embeddings are projected for better visualization.

we show to be beneficial in Sec. 5.3, especially when the hyperbolic manifold is set to be the latent space.

### 3.3. Latent Spaces

We propose to consider three diverse manifolds for embedding the input sequences. In fact, the objective of Eq. 2 forces the model to focus on features corresponding to common characters in the embeddings extracted from the encoder and to iteratively reduce their distances from a center. As a result, the method relies on a metric which, in turn, depends on the metric space  $\mathcal{L}$  chosen as the latent space. Motivated by this, we are the first to define the same objective on three manifolds, each with its own specific metric: the *Euclidean space*  $\mathbb{R}^n$ , the *spherical space*  $\mathbb{S}^n \subset \mathbb{R}^{n+1}$ , and the *hyperbolic space*  $\mathbb{H}^n \subset \mathbb{R}^{n+1}$ . These spaces have a different curvature that causes the distance to behave differently in each manifold.

#### 3.3.1. Euclidean Latent Space

When  $\mathcal{L} = \mathbb{R}^n$ , the distance coincides with the  $L^2$  metric  $d_E(x, y) = \|x - y\|_2$ , and the model is defined substituting the distance  $d$  with  $d_E$  in Eq. 2.

### 3.3.2. $n$ -Sphere Latent Space

With  $\mathcal{L} = \mathbb{S}^n$ , we modify the proposed COSKAD model, building on top of the  $S$ -VAE presented in [35]. We dub the model *COSKAD-radial* since it constrains inputs onto the spherical surface with a fixed radius  $\mathbb{S}^n = \{x \in \mathbb{R}^{n+1} : \|x\|_2 = 1\}$ ; the posterior of the normal data approximates a Power Spherical distribution  $q_X(x; \mu, \kappa)$  [36], with a constraint  $L_{dir} = \frac{1}{N} \sum_{i=1}^N (1 - x \cdot c)$  to push the samples close to the empirical mean direction  $c$ . The target loss is  $L = \gamma L_{rec} + \phi L_{dir} + \beta L_{KL}$ , where  $L_{rec}$  defines the objective for the Variational AutoEncoder reconstruction,  $L_{KL}$  is the Kullback-Leibler divergence,  $\gamma, \phi, \beta \in \mathbb{R}$  hyperparameters. The anomaly score is solely given by the *cosine distance* between any sample  $x$  on  $\mathbb{S}^n$  and the empirical mean  $c$  computed at train time.

### 3.3.3. Hyperbolic Latent Space

When  $\mathcal{L} = \mathbb{H}^n$ , we model it with the *Poincaré Ball* which coincides with the unit euclidean open ball  $\mathbb{D}^n$  endowed with the Riemmanian metric

$$g_x^{\mathbb{D}} = \frac{2I^n}{1 - \|x\|^2},$$

where  $I^n$  represents the Identity matrix. This metric tensor induces the distance

$$d_{\mathbb{D}}(x, y) = \operatorname{arcosh} \left( 1 + \frac{2\|x - y\|^2}{(1 - \|x\|^2)(1 - \|y\|^2)} \right). \quad (3)$$

The distances between the points on this manifold increase exponentially with distance from the origin  $O$ . To take full advantage of this property, we let the cluster center move in the Poincaré Ball in a data-driven fashion, but we also experienced defining the center as a fixed point, as detailed in Sec. 5.3. In Fig. 3, comparing the Euclidean (a) with the hyperbolic (c) case, the effect of this distance is shown: in the Euclidean case, farther points tend to be more spread since the hyperbolic distance  $d_{\mathbb{D}}$  ensures a stronger attraction towards the center, i.e.  $d_{\mathbb{D}}$  grows exponentially with the distance from the center. In this case, the model is obtained from COSKAD by adding a projection layer  $\exp_0 : \mathbb{R}^{n+1} \rightarrow \mathbb{D}^n$ , which performs the exponential mapping to get the hyperbolic representation in  $\mathbb{D}^n$ . Thus, the objective defined in Eq. 2 becomes:

$$\min_{\mathcal{W}} \frac{1}{N} \sum_{i=1}^N d_{\mathbb{D}}(\text{exp}_0(\Phi(x_i, \mathcal{W})), c) + \alpha f(\mathcal{W}). \quad (4)$$

### 3.4. Anomaly Score

At inference time, the anomaly score  $s$  for each sample  $x$  (representing a single agent in a time window composed by  $T$  frames  $\{f_1, f_2, \dots, f_T\}$ ) is defined as the distance of its COSKAD embedding from the center  $c$ :

$$s(x) = d(\Phi(x, \mathcal{W}), c). \quad (5)$$

To score a single frame  $\bar{f}$ , for each agent  $p$ , we first collect all the windows involving  $p$  in a set  $w^p$ , and we restrict this set picking only the windows containing  $\bar{f}$  to a set  $w_{\bar{f}}^p$ . Then, we calculate the score through Eq. 5 and thus set the score for  $p$  at frame  $\bar{f}$  to be the mean of those scores:

$$s^p(\bar{f}) = \frac{1}{|w_{\bar{f}}^p|} \sum_{x \in w_{\bar{f}}^p} s(x). \quad (6)$$

Finally, we get the score for a single frame  $\bar{f}$  by a max pooling operation over all the agents present in the scene at frame  $\bar{f}$ :

$$s(\bar{f}) = \max_{p \in P_{\bar{f}}} \{s^p(\bar{f})\}, \quad (7)$$

where  $P_{\bar{f}}$  is the collection of all the people present in the clip at frame  $\bar{f}$ .

## 4. Experiments

In this section, we evaluate the performance of COSKAD on the human-related versions of three established benchmarks against state-of-the-art skeleton-based methods. Next, we discuss how our approach relates to techniques that additionally employ appearance. The section is organized as follows: first, we illustrate the datasets and the metric (Sec. 4.1). Then, we describe the results of the experiments and discuss the performance (Sec. 4.2). The last part of this section provides details about the implementation and data preprocessing (Sec. 4.3).

Dataset	# frames					
	Total	Training	Validation	Test	Normal	Abnormal
Avenue [17]	43,499	28,175	-	15,324	25,891	17,608
STC [13]	317,398	274,515	-	42,883	300,308	17,090
UBnormal [18]	236,902	116,087	28,175	92,640	147,887	89,015
HR-Avenue [9]	42,883	28,175	-	14,708	25,891	16,992
HR-STC [9]	313,212	274,515	-	38,697	297,090	16,122
HR-UBnormal ( <i>Proposed</i> )	234,751	116,087	28,175	90,489	147,887	86,864

Table 1: Overview of the three datasets chosen, CUHK Avenue, ShanghaiTech Campus, and UBnormal, as well as their human-related versions.

#### 4.1. Benchmarks

The following sections describe the datasets and introduce the metric we use to score anomalous frames in a video sequence.

##### 4.1.1. Datasets

**UBnormal.** UBnormal [18] is the largest and most recent dataset for frame-level video anomaly detection, the only one to provide *train-validation-test* splits that adhere to the *Open Set* protocol, i.e., the sets of anomalous events for train, validation, and test are disjoint. It consists of 19 clips, which encompass both normal and abnormal events, for each of the 29 diverse background scenes. UBnormal has several distinctive features. First, as illustrated in Table 1, it contains more anomalous frames than those presented in CUHK Avenue or ShanghaiTech Campus. Additionally, it has labels for each anomaly at both the frame and pixel level, with annotations describing the anomalous actions (e.g., jumping, sleeping, stealing). UBnormal exhibits a larger list of anomalous event types than previous Video Anomaly Detection datasets: it includes 22 categories of anomalies, in contrast to ShanghaiTech Campus and CUHK Avenue which only encompass 11 and 5, respectively. Additionally, it introduces a variety of objects, such as cars and bicycles, to both the train and the test sets to avoid the anomaly being detected because the object was not seen during the

training phase. In contrast to other benchmarks, it is synthetic and its virtual 3D scenes are created with Cinema4D with heterogeneous 2D backgrounds (e.g., streets, train stations, and office rooms, with different viewpoints and lighting conditions). Since COSKAD is trained in the OCC framework, we extract only the normal sample poses from the training set. Conversely, we maintain the original validation and test split in this setting.

**HR-UBnormal (*Proposed*).** We propose HR-UBnormal as an extension of the original UBnormal dataset with kinematic motion representations and a selected set of anomalies that relate only to human behaviors. AlphaPose [20] is first used to extract the poses, and PoseFlow [21] is used to track the skeletons throughout each video. We then filter out the non-human related anomalies. We remove the sub-sequences in which the only anomalous object was not a person (e.g., a car) or the anomaly cannot be detected using only body poses (e.g., fire in the scene). See supplementary materials for the list of deleted non-HR anomalous actions. As a result, we leave the validation set unaltered while eliminating the frames 2.32% of the test set. Table 1 lists the total number of normal and abnormal frames.

**CUHK Avenue.** The CUHK Avenue dataset [17] contains 16 training videos and 21 testing videos with a total of 47 abnormal events recorded with different camera positions and angles. The HR-version [9] is obtained by removing frames where (1) the anomalous event is non-human, (2) the person involved is occluded, or (3) the main subject cannot be detected and tracked.

**ShanghaiTech Campus.** The ShanghaiTech Campus (STC) dataset [13] contains footage from 13 cameras around the campus with different light conditions and camera angles. It contains more than 300,000 total frames, and there are 130 abnormal events, some of which are not present in other datasets (e.g., chasing, brawling). The HR-version [9] is obtained by removing 6 out of 107 test videos where the anomalous event is non-human.

#### 4.1.2. Evaluation metric

We score each frame in a video as mentioned in Sec. 3.4. Then we compare it with the ground-truth labels to compute the *Area Under the Curve* (AUC) score, following the previous literature in Video AD [7, 9, 10, 17, 18, 37].

#### 4.2. Comparison with SoA

We compare COSKAD against relevant skeleton-based state-of-the-art techniques on the HR version of the selected three datasets. This comparison, considering skeleton-based anomaly detection algorithms, is described in Sec. 4.2.1 and regards the bottom part of Table 2. Then, Sec. 4.2.2 compares skeleton-based Vs. video-based techniques, and it discusses progress on the two fronts.

##### 4.2.1. Comparison with skeleton-based techniques

Table 2 reports the results of the experiments we have conducted on HR-UBnormal, HR-ShanghaiTech Campus, and HR-Avenue. On HR-UBnormal, all three proposed volume shrinking strategies of COSKAD introduced in Sec. 3.3 outperform the current best [9]. In particular, our best variant, COSKAD-*hyperbolic*, outperforms [9] by a relative improvement of 7% (65.5 AUC Vs 61.2 AUC). This remarks on the effectiveness of COSKAD in the case of the challenging open set anomalies of UBnormal.

The HR-ShanghaiTech Campus and HR-Avenue rankings are tighter; still, COSKAD-*Euclidean* attains the best performance on both datasets, setting a new state-of-the-art on these benchmarks. Although the performance gain between COSKAD-*Euclidean* (77.1 and 87.8) and the current best skeleton-based method of [8] (76.5, 87.3) is relatively small, it should be noted that, even compared to skeleton-based baselines, our model remains lightweight (cf. the parameter count in Table 2). Comparing the three COSKAD versions, the *radial* approach underperforms. This might be a consequence of the more dispersed distribution of the embeddings from the center, as visible in Fig. 3.

	<b>Video-based methods</b>	<b>Params</b>	<b>UBnormal</b>	<b>STC</b>	<b>Avenue</b>
<i>S</i>	Sultani <i>et al.</i> [2]	-	50.3	-	-
	Georgescu <i>et al.</i> [37]	> 80M	61.3	-	-
	Bertasius <i>et al.</i> [38]	121M	68.5	-	-
<i>WS</i>	Georgescu <i>et al.</i> [37]	> 80M	59.3	82.7	92.3
<i>OCC</i>	Hasan <i>et al.</i> [6]	-	-	70.4	80.0
	Park <i>et al.</i> [39]	-	-	69.8	82.8
	Liu <i>et al.</i> [7]	14M	-	72.8	85.1
	Chang <i>et al.</i> [40]	-	-	73.3	86.0
	Barbalau <i>et al.</i> [41]	> 80M	62.5	83.8	93.7
	<b>Skeleton-based methods</b>	<b>Params</b>	<b>HR-UBnormal</b>	<b>HR-STC</b>	<b>HR-Avenue</b>
<i>OCC</i>	Morais <i>et al.</i> [9]	25K	61.2	75.4	86.3
	Markovitz <i>et al.</i> [10]	805K	55.2	74.8	58.1
	Luo <i>et al.</i> [8]	8M	-	<u>76.5</u>	<u>87.3</u>
	Ours - <i>radial</i>	285K	63.4	75.2	82.2
	Ours - <i>Euclidean</i>	240K	<u>65.2</u>	<b>77.1</b>	<b>87.8</b>
	Ours - <i>hyperbolic</i>	240K	<b>65.5</b>	75.6	<u>87.3</u>

Table 2: Results on the human-related versions of the datasets UBnormal (*HR-UBnormal*), ShanghaiTech Campus (*HR-STC*) and CUHK Avenue (*HR-Avenue*), measured in terms of AUC score (bottom part of the table). We highlight in bold the best results and underline the second best. We report the results of video-based models on the non-HR versions of the aforementioned datasets (upper part of the table); it should be noted that such methods cannot be directly compared with skeleton-only ones, which are rather complementary, and hence are displayed in gray. The blocks split the table according to each method’s framework, where *S*, *WS* and *OCC* stand for *Supervised*, *Weakly-Supervised* and *One Class Classification* methods, respectively.

#### 4.2.2. Relation of COSKAD with video-based methods

For completeness, the upper part of Table 2 reports video-based techniques, tested on the complete set of videos of *UBnormal*, *ShanghaiTech Campus* and *CUHK Avenue*. The complete datasets include human-related anomalies, as well as anomalies not relating to people (e.g., crashing cars) and only stemming from visual cues, such as fire, smoke, and fog. The general video-based anomaly detection techniques in the top part of Table 2 have access to the spatio-temporal volume of RGB-pixel information, accounting for appearance

(color, shape, object-like, etc.) and motion cues (e.g., optical flow). On the other hand, skeletal motion accounts for a small subset of the information contained in videos, but it condenses cues about the actions, avoiding misleading features such as lightning conditions or viewing directions. Indeed, even without the ability to detect non-human events, our model achieves 65.0 AUC (cf. Table 3). In contrast, the current state-of-the-art OCC video-based model [41] only scores an AUC of 62.5. Besides, COSKAD only uses a fraction of parameters of [41], namely 240K Vs. 80M (−99.7%). On *ShanghaiTech Campus* and *CUHK Avenue*, our best-performing model reports an AUC score of 74.3 and 85.7, respectively, and only [34, 41] surpass COSKAD’s performance. Overall, our models’ high performance and reduced complexity suggest that skeleton-based techniques could be a valuable research direction to complement appearance-based cues. Moreover, by solely processing motion, as COSKAD does, additional privacy and fairness guarantees are provided, as the model cannot exploit biases related to skin color, gender, or clothing style.

#### 4.3. Experimental setup

**Implementation details.** We train our proposed COSKAD with PyTorch Lightning using two Nvidia P6000 GPUs for 80 epochs, with a learning rate of 0.0001 and ADAM [42] optimizer. The training phase required 1.5 hours, which is a fraction of the training time of [9, 10]. We consider  $V = 17$  key points to represent a pose and divide each agent’s motion history by adopting a sliding window procedure (each window has a length of  $T = 12$  frames with stride 1 so that windows overlap).

**Pose normalization.** Since the 2D positions of the joints refer to the frame, we normalize the poses to make them independent of the spatial location, following [9]. For all the datasets, we perform an additional normalization stage by applying robust scaling to reduce the contribution of outliers, as also done in [9].

## 5. Ablation Studies

In this section, we report additional results and experiments that have guided us in building COSKAD. This study focuses on establishing the two main components of the proposed model and compares two strategies concerning the center update and the scoring method. All the experiments presented in this section are performed on the established UBnormal dataset and are conducted using the best-performer Euclidean and the hyperbolic versions of COSKAD. Notably, each model’s variant with an STS-GCN encoder presented in this section outperforms all the OCC techniques reported in Table 2.

### 5.1. Encoder

As illustrated in Sec. 3.1, COSKAD is equipped with a separable GCN-Encoder to process the input graphs. The first to propose a GCN as a kinematic encoder in the context of anomaly detection was [8], while previous works rely on LSTM [43], such as [9]. For this reason, we compare our encoder with other established GCN architectures, such as a plain GCN [30] and the ST-GCN [12], which have been employed in [8, 10]. As reported in Table 3, the selected separable GCN attains the best results among competitors, showing an increase in performance of 9.8% and 10.2% over GCN [30] and 3.6% and 7.8% over ST-GCN [12] on the Euclidean and hyperbolic models, respectively. This result confirms that separating the kinematic adjacency matrix in its spatial and temporal parts allows for improved input representations. Moreover, separating the adjacency matrix results in a significant reduction in parameters, yielding an encoder with only 31K parameters against 75K and 170K of {ST-GCN, GCN}-based encoders, respectively.

### 5.2. Projector

The importance of the projector when dealing with representations and metric objectives has been studied thoroughly in the field of SSL [15, 16]. Following [15], we compare three different definitions for the projector: the *Identity* (no projector), *Linear* (two linear layers), and *Non-Linear* (one block of linear

Encoder			Projector			Center Update		Hyperbolic	UBnormal	
GCN[30]	ST-GCN[12]	Sep. GCN	Identity	Linear	Non-Linear	Static	Dynamic		Valid.	Test
✓					✓		✓		68.9	59.1
✓					✓		✓	✓	69.1	59.0
	✓				✓		✓		68.4	62.6
	✓				✓		✓	✓	72.3	60.3
		✓	✓			✓			72.7	64.5
		✓	✓			✓		✓	72.0	63.6
		✓	✓				✓		71.3	64.7
		✓	✓				✓	✓	72.9	64.5
		✓		✓		✓			69.8	64.2
		✓		✓			✓	✓	71.1	64.7
		✓			✓	✓			74.5	64.6
		✓			✓	✓		✓	74.0	63.1
		✓			✓		✓		75.8	64.9
		✓			✓		✓	✓	<b>76.4</b>	<b>65.0</b>

Table 3: Ablation on the components of the proposed method COSKAD. Red checkmarks indicate the technical choices we implement in the final model. The results are attained on the UBnormal dataset.

layer, non-linearity, and Batch Normalization [33] followed by another linear layer) projectors. In Table 3, we empirically confirm the results of [15], showing that a non-linear projector provides a boost in performance (+5.6%, +0.54% on validation and test, respectively) when compared to an Identity projector, i.e., directly using the output of the encoder. The Identity and Linear strategies provide similar results, showing that a non-linearity is needed to improve the representations in the latent space. As a further investigation, we also verify the deepness of the non-linear projector module. Specifically, we assess our model against different versions of it with a naive non-linear decoder without any block, performing only Batch Normalization, a ReLU activation and a linear layer, and a deeper projector involving two non-linear blocks followed by a linear layer. As depicted in Table 4, a single non-linear block considerably increases performance, especially in the hyperbolic setting (+2%). Since the COSKAD’s modules operate in Euclidean spaces, this result is not surprising and exposes the need for a projector when dealing with non-Euclidean latent spaces. Further, using more layers results in a slight degradation in performance when using either the Euclidean or the hyperbolic latent space (−0.2%, −0.6%,

# Blocks	Euclidean		Hyperbolic	
	Validation	Test	Validation	Test
0	71.2	64.1	72.4	63.7
1	75.8	64.9	<b>76.4</b>	<b>65.0</b>
2	75.7	64.8	74.01	64.6

Table 4: Ablation on the depth of the Non-Linear projector proposed (cf. Sec.5.2).

respectively).

### 5.3. Center Update Strategy

Since the metric objective of our method seeks to minimize the distance between the latent representations and a point defined in the latent space, it is critical to choose the optimal rule to update the center position during training to achieve optimal mapping. [19] proposed to fix a point in the latent space and then perform training around it. We experiment with this method, dubbed *Static*, and compare it with a novel rule to update the center position, dubbed *Dynamic*, in Table 3. As can be seen, the *Dynamic* strategy provides the best result, especially in the hyperbolic space, with an increase of 3% wrt to its *Static* counterpart, while the gain in the Euclidean space (+0.4%) is more marginal. We expected a similar behavior since the metric defined within the Poincaré Ball induces a distance that grows exponentially with the radius, therefore, when the learning center is left free to move, the model can take advantage of it. On the other hand, with the *Static* strategy, it can be challenging for the model to minimize the distances between the embeddings and the fixed center.

### 5.4. COSKAD AutoEncoder

We also consider a multi-task learning objective for COSKAD coupling the original objective illustrated in Eq. 2 with a reconstruction error; to do this, we included an additional module that acts as a decoder, allowing COSKAD to reconstruct the original poses. Altogether, this makes our proposed model a GCN AutoEncoder, dubbed COSKAD-AE, and the new module has been

Model	Training	Inference	UBnormal
COSKAD	$L_{hyp}$	$s_{hyp}$	64.9
		$s_{rec}$	63.0
COSKAD-AE	$L_{hyp} + L_{rec}$	$s_{hyp}$	64.1
		$s_{hyp} + s_{rec}$	63.4

Table 5: Performance evaluation of our proposed models with COSKAD-AE. AUC score is reported for the UBnormal dataset.

obtained by reversing the GCN-Encoder. Table 5 compares the performance of COSKAD-AE, trained with both reconstruction and hypersphere loss, against our best model. Three methods for calculating the anomaly score are possible: either the reconstruction or hypersphere loss can be employed alone (named  $s_{rec}$  and  $s_{hyp}$ , respectively in Table 5), or the two scores can be combined ( $s_{rec} + s_{hyp}$ ). The best performances are achieved by the only hypersphere score. This is probably due to the Separable GCN-Encoder that, separately learning the trajectories of single joints and unified poses for each timeframe, exposes improved generalization that affects  $s_{rec}$  and provides better reconstructions.

## 6. Conclusion

We have proposed a novel Skeleton-based anomaly detection method based on the minimization of latent vectors to a center, exploiting the properties of three different manifolds: Euclidean, hyperbolic, and spherical. We defined the minimization metrics and scoring and investigated the alterations in space induced by manifolds. By leveraging an STS-GCN encoder and coupling it with a loss that matches the OCC objective, COSKAD outperforms SoA models on established human-related benchmarks. On the most recent and challenging HR-UBnormal, all three versions of the proposed COSKAD reach SoA performance, which shows the representational power of our approach.

## References

- [1] V. Chandola, A. Banerjee, V. Kumar, Anomaly detection: A survey, *ACM computing surveys (CSUR)* 41 (3) (2009) 1–58.
- [2] W. Sultani, C. Chen, M. Shah, Real-world anomaly detection in surveillance videos, in: *Proceedings of the IEEE/CVF Conference on Computer Vision and Pattern Recognition (CVPR)*, 2018, pp. 6479–6488.
- [3] B. Prenkaj, D. Aragona, A. Flaborea, F. Galasso, S. Gravina, L. Podo, E. Reda, P. Velardi, A self-supervised algorithm to detect signs of social isolation in the elderly from daily activity sequences, *Artificial Intelligence in Medicine* 135 (2023) 102454. doi:<https://doi.org/10.1016/j.artmed.2022.102454>.  
URL <https://www.sciencedirect.com/science/article/pii/S0933365722002068>
- [4] D. J. Atha, M. R. Jahanshahi, Evaluation of deep learning approaches based on convolutional neural networks for corrosion detection, *Structural Health Monitoring* 17 (5) (2018) 1110–1128.
- [5] Y. Liu, S. Chawla, Social media anomaly detection: Challenges and solutions, in: *Proceedings of the 21th ACM SIGKDD International Conference on Knowledge Discovery and Data Mining*, 2015, pp. 2317–2318.
- [6] M. Hasan, J. Choi, J. Neumann, A. K. Roy-Chowdhury, L. S. Davis, Learning temporal regularity in video sequences, in: *Proceedings of the IEEE/CVF Conference on Computer Vision and Pattern Recognition (CVPR)*, 2016, pp. 733–742.
- [7] W. Liu, W. Luo, D. Lian, S. Gao, Future frame prediction for anomaly detection—a new baseline, in: *Proceedings of the IEEE/CVF Conference on Computer Vision and Pattern Recognition (CVPR)*, 2018, pp. 6536–6545.

- [8] W. Luo, W. Liu, S. Gao, Normal graph: Spatial temporal graph convolutional networks based prediction network for skeleton based video anomaly detection, *Neurocomputing* 444 (2021) 332–337.
- [9] R. Morais, V. Le, T. Tran, B. Saha, M. Mansour, S. Venkatesh, Learning regularity in skeleton trajectories for anomaly detection in videos, in: *Proceedings of the IEEE/CVF conference on computer vision and pattern recognition*, 2019, pp. 11996–12004.
- [10] A. Markovitz, G. Sharir, I. Friedman, L. Zelnik-Manor, S. Avidan, Graph embedded pose clustering for anomaly detection, in: *Proceedings of the IEEE/CVF Conference on Computer Vision and Pattern Recognition (CVPR)*, 2020, pp. 10539–10547.
- [11] S. Xu, Y.-X. Wang, L.-Y. Gui, Diverse human motion prediction guided by multi-level spatial-temporal anchors, in: *European Conference on Computer Vision (ECCV)*, 2022, pp. 251–269.
- [12] S. Yan, Y. Xiong, D. Lin, Spatial temporal graph convolutional networks for skeleton-based action recognition, *Proceedings of the AAAI Conference on Artificial Intelligence* 32 (Apr. 2018). doi:10.1609/aaai.v32i1.12328. URL <https://ojs.aaai.org/index.php/AAAI/article/view/12328>
- [13] W. Luo, W. Liu, S. Gao, A revisit of sparse coding based anomaly detection in stacked rnn framework, in: *Proceedings of the IEEE/CVF Conference on Computer Vision and Pattern Recognition (CVPR)*, 2017, pp. 341–349.
- [14] T. Sofianos, A. Sampieri, L. Franco, F. Galasso, Space-time-separable graph convolutional network for pose forecasting, in: *2021 IEEE/CVF International Conference on Computer Vision (ICCV)*, 2021, pp. 11209–11218.
- [15] T. Chen, S. Kornblith, M. Norouzi, G. Hinton, A simple framework for contrastive learning of visual representations (2020). doi:10.48550/ARXIV.

2002.05709.

URL <https://arxiv.org/abs/2002.05709>

- [16] J. Grill, F. Strub, F. Alché, C. Tallec, P. H. Richemond, E. Buchatskaya, C. Doersch, B. Á. Pires, Z. D. Guo, M. G. Azar, B. Piot, K. Kavukcuoglu, R. Munos, M. Valko, Bootstrap your own latent: A new approach to self-supervised learning, CoRR abs/2006.07733 (2020). [arXiv:2006.07733](https://arxiv.org/abs/2006.07733).  
URL <https://arxiv.org/abs/2006.07733>
- [17] C. Lu, J. Shi, J. Jia, Abnormal event detection at 150 fps in matlab, in: Proceedings of the IEEE/CVF Conference on Computer Vision and Pattern Recognition (CVPR), 2013, pp. 2720–2727.
- [18] A. Acintoae, A. Florescu, M.-I. Georgescu, T. Mare, P. Sumedrea, R. T. Ionescu, F. S. Khan, M. Shah, Ubnormal: New benchmark for supervised open-set video anomaly detection, in: Proceedings of the IEEE/CVF Conference on Computer Vision and Pattern Recognition (CVPR), 2022, pp. 20143–20153.
- [19] L. Ruff, R. Vandermeulen, N. Goernitz, L. Deecke, S. A. Siddiqui, A. Binder, E. Müller, M. Kloft, Deep one-class classification, in: Proceedings of the International Conference on Machine Learning (ICML), 2018, pp. 4393–4402.
- [20] H.-S. Fang, S. Xie, Y.-W. Tai, C. Lu, Rmpe: Regional multi-person pose estimation, in: ICCV, 2017, pp. 2334–2343.
- [21] Y. Xiu, J. Li, H. Wang, Y. Fang, C. Lu, Pose Flow: Efficient online pose tracking, in: BMVC, 2018.
- [22] D. Bogdoll, M. Nitsche, J. M. Zöllner, Anomaly detection in autonomous driving: A survey, in: Proceedings of the IEEE/CVF Conference on Computer Vision and Pattern Recognition (CVPR), 2022, pp. 4488–4499.
- [23] W. Hilal, S. A. Gadsden, J. Yawney, Financial fraud: A review of anomaly detection techniques and recent advances, *Expert Syst. Appl.* 193 (C) (may

2022).

URL <https://doi.org/10.1016/j.eswa.2021.116429>

- [24] F. Jiang, J. Yuan, S. A. Tsafaris, A. K. Katsaggelos, Anomalous video event detection using spatiotemporal context, *Comput. Vis. Image Underst.* (2011) 323–333.  
URL <https://doi.org/10.1016/j.cviu.2010.10.008>
- [25] S. Calderara, U. Heinemann, A. Prati, R. Cucchiara, N. Tishby, Detecting anomalies in people’s trajectories using spectral graph analysis, *Comput. Vis. Image Underst.* (2011).
- [26] D. Gong, L. Liu, V. Le, B. Saha, M. R. Mansour, S. Venkatesh, A. Van Den Hengel, Memorizing normality to detect anomaly: Memory-augmented deep autoencoder for unsupervised anomaly detection, in: *2019 IEEE/CVF International Conference on Computer Vision (ICCV)*, 2019, pp. 1705–1714. doi:10.1109/ICCV.2019.00179.
- [27] D. M. Tax, R. P. Duin, Support vector data description, *Machine learning* (2004).
- [28] Z. Wang, Z. Chen, J. Ni, H. Liu, H. Chen, J. Tang, Multi-scale one-class recurrent neural networks for discrete event sequence anomaly detection, in: *Proceedings of the 27th ACM SIGKDD Conference on Knowledge Discovery & Data Mining*, 2021, pp. 3726–3734.
- [29] M. Sabokrou, M. Fayyaz, M. Fathy, R. Klette, Deep-cascade: Cascading 3d deep neural networks for fast anomaly detection and localization in crowded scenes, *IEEE Transactions on Image Processing* 26 (2017) 1992–2004.
- [30] T. N. Kipf, M. Welling, Semi-Supervised Classification with Graph Convolutional Networks, in: *Proceedings of the International Conference on Learning Representations, ICLR ’17*, 2017.
- [31] C. Zhong, L. Hu, Z. Zhang, Y. Ye, S. Xia, Spatio-temporal gating-adjacency gcn for human motion prediction, in: *Proceedings of the IEEE/CVF Con-*

- ference on Computer Vision and Pattern Recognition (CVPR), 2022, pp. 6447–6456.
- [32] Y.-F. Song, Z. Zhang, C. Shan, L. Wang, Constructing stronger and faster baselines for skeleton-based action recognition, *IEEE Transactions on Pattern Analysis and Machine Intelligence* (2022) 1–doi:10.1109/TPAMI.2022.3157033.
- [33] S. Ioffe, C. Szegedy, Batch normalization: Accelerating deep network training by reducing internal covariate shift, in: F. Bach, D. Blei (Eds.), *Proceedings of the 32nd International Conference on Machine Learning (ICML)*, Vol. 37, 2015, pp. 448–456.
- [34] M.-I. Georgescu, A. Bărbălău, R. T. Ionescu, F. Shahbaz Khan, M. Popescu, M. Shah, Anomaly detection in video via self-supervised and multi-task learning, in: *Proceedings of the IEEE/CVF Conference on Computer Vision and Pattern Recognition (CVPR)*, 2021, pp. 12737–12747.
- [35] T. R. Davidson, L. Falorsi, N. De Cao, T. Kipf, J. M. Tomczak, Hyperspherical variational auto-encoders, *34th Conference on Uncertainty in Artificial Intelligence (UAI-18)* (2018).
- [36] N. De Cao, W. Aziz, The power spherical distribution, *Proceedings of the 37th International Conference on Machine Learning, INNF+* (2020).
- [37] M. I. Georgescu, R. Ionescu, F. S. Khan, M. Popescu, M. Shah, A background-agnostic framework with adversarial training for abnormal event detection in video, *IEEE Transactions on Pattern Analysis and Machine Intelligence* (2021). doi:10.1109/TPAMI.2021.3074805.
- [38] G. Bertasius, H. Wang, L. Torresani, Is space-time attention all you need for video understanding?, in: *Proceedings of the International Conference on Machine Learning (ICML)*, 2021, p. 4.

- [39] H. Park, J. Noh, B. Ham, Learning memory-guided normality for anomaly detection, in: Proceedings of the IEEE/CVF conference on computer vision and pattern recognition, 2020, pp. 14372–14381.
- [40] Y. Chang, Z. Tu, W. Xie, J. Yuan, Clustering driven deep autoencoder for video anomaly detection, in: Computer Vision–ECCV 2020: 16th European Conference, Glasgow, UK, August 23–28, 2020, Proceedings, Part XV 16, Springer, 2020, pp. 329–345.
- [41] A. Barbalau, R. T. Ionescu, M.-I. Georgescu, J. Dueholm, B. Ramachandra, K. Nasrollahi, F. S. Khan, T. B. Moeslund, M. Shah, Ssmtl++: Revisiting self-supervised multi-task learning for video anomaly detection, *Computer Vision and Image Understanding* 229 (2023) 103656. doi:<https://doi.org/10.1016/j.cviu.2023.103656>.  
URL <https://www.sciencedirect.com/science/article/pii/S107731422300036X>
- [42] D. P. Kingma, J. Ba, Adam: A method for stochastic optimization, *CoRR* abs/1412.6980 (2015).
- [43] S. Hochreiter, J. Schmidhuber, Long short-term memory, *Neural Computation* 9 (8) (1997) 1735–1780. doi:10.1162/neco.1997.9.8.1735.

*Alessandro Flaborea.* is a Ph.D. student at the Sapienza University of Rome. He received his degree in Computer Science from the University of Udine, Italy, and his master’s degree in Data Science from the Sapienza University of Rome. His research interests include few-shot learning, time series, video anomaly detection, and pose estimation.

*Guido Maria D’Amely di Melendugno.* is a Ph.D. student in Computer Science at the Sapienza University of Rome. After the master’s degree in Mathematics obtained at the Sapienza University of Rome, he focused on Computer Vision. His research interests lie in Text-Image Retrieval, Multimodal CV, Pose Forecasting, and Video Anomaly Detection.

*Stefano D'Arrigo.* is a Ph.D. student in Artificial Intelligence at the Sapienza University of Rome. He received a BSc in Computer Science at the University of Catania, Italy, and a MSc in Data Science at the Sapienza University of Rome. His research interests include pose estimation, video anomaly detection, and geometric deep learning.

*Marco Aurelio Sterpa.* is an MSc student at the Sapienza University of Rome. He received his bachelor's degree in Computer Science from the Sapienza University of Rome and is currently a second-year master's degree student in Data Science. His research interests include time series and video anomaly detection.

*Alessio Sampieri.* is a Ph.D. student in Data Science at the Sapienza University of Rome. He received his degree in Statistics for Management and master's degree in Data Science from the Sapienza University of Rome. His research interests include human motion and its forecasting, video analysis and understanding and geometric deep learning.

*Fabio Galasso.* heads the Perception and Intelligence Lab (PINLab) at the Dept. of Computer Science, Sapienza University of Rome (Italy).

His research interests include distributed and multi-agent intelligent systems, perception (detection, recognition, re-identification, forecasting) and general intelligence (reasoning, meta-learning, domain adaptation), within sustainable (low-power-consumption and constrained-computational-resource sensors and devices) and interpretable frameworks.